# Gut Dysbiosis and Carbamazepine Differentially Impact Hippocampal Glial Response and Neurodegeneration in a Viral Infection-Induced Seizure Model

**Authors:** Sophia Shonka, PhD[1], Inga Erickson, MS[1], and Melissa Barker-Haliski, PhD[1]*

1- Department of Pharmaceutics, University of Washington, Seattle, WA

* Corresponding author contact information: mhaliski@uw.edu; phone: 206-221-4939

**Abstract**

**Objective**: Brain infection is an underrecognized global cause of epilepsy due to the ensuing neuroinflammation and neurological damage. Immune system response, including underlying neuroinflammation, is dynamically shaped by the intestinal microbiome. In experimental rodent epilepsy models, seizure burden and antiseizure medication (ASM) activity can be dramatically influenced by gut dysbiosis, including in the Theiler's murine encephalomyelitis virus (TMEV) infection model of acute symptomatic seizures and long-term epilepsy. We previously demonstrated that experimentally induced gut dysbiosis via repeated antibiotic administration alters seizure burden and carbamazepine (CBZ) anticonvulsant activity in this model (1). However, whether dysbiosis and CBZ differentially shape neuropathological damage and neuroinflammation following TMEV infection was not reported.

**Methods**: Here, we extended our earlier study to quantify the extent to which antibiotic-induced gut dysbiosis and repeated CBZ administration during TMEV infection altered the severity of acute neuropathology. Hippocampal tissue was analyzed 7 days post-infection using quantitative immunofluorescence to assess neuronal death, microglial and astroglial reactivity, and neuronal proliferation across CA1, CA3, and dentate gyrus (DG) subregions.

**Results**: Dysbiosis markedly exacerbated hippocampal neurodegeneration and gliosis, accompanied by increased glial proliferation, whereas CBZ administration reversed these effects in a hippocampal region-dependent manner. Collectively, these findings demonstrate that the gut microbiome primes hippocampal neuroimmune responses to viral infection-induced acute seizures and modifies associated neuropathology in a hippocampal region-specific manner.

**Significance**: This work identifies the gut-brain axis as a critical determinant of neuroinflammatory damage after infection-induced symptomatic seizures, highlighting the gut

microbiome as a potential therapeutic target to alleviate the worldwide epilepsy burden.

**Keywords:** Carbamazepine, neuroinflammation, neurodegeneration, microbiome, astrogliosis, microgliosis

## Highlights

- Experimentally-evoked gut dysbiosis exacerbates hippocampal neurodegeneration after brain viral infection.
- Experimentally-evoked gut dysbiosis increases microgliosis and glial proliferation after brain viral infection.
- Carbamazepine reversed dysbiosis-induced neuroinflammation and neurodegeneration.
- Experimentally-evoked gut dysbiosis differentially modulates glial response in the dentate gyrus.

## Introduction

Epilepsy is an underrecognized long-term complication of central nervous system (CNS) infection-induced encephalitis (2), increasing epileptogenesis risk up to 22-fold (3–5). Importantly, low sociodemographic index nations carry a higher burden of CNS infection-induced acquired epilepsy risk (e.g., 37% of cases in Mali (6) vs 5.8% in the United States (7)). Thus, viral infection-induced encephalitis is a unique risk factor that disproportionately contributes to the global burden of epilepsy. However, rodent models of encephalitis-induced acute symptomatic seizures (ASyS) and acquired epilepsy are less frequently integrated into preclinical epilepsy research. One translationally relevant rodent model is induced through Theiler's murine encephalomyelitis virus (TMEV) infection directly into the CNS. This leads to ASyS in 60% of C57BL/6J mice, of which, 50% develop spontaneous recurrent seizures (SRS) (3,8,9). Mice also display similar behavioral comorbidities (10–13), and neuropathology (3,12–15) observed in clinical cases. This model is especially advantageous due to the lower mortality rate observed in other viral encephalitis-induced epilepsy models (3,8). Thus, the TMEV mouse model is an etiologically relevant model of viral infection-induced ASyS that encapsulates multiple clinical features and fills an important gap to address the global epilepsy burden.

Neuroinflammation is a key mediator of acute and chronic seizures (16–18) and neuropathology following viral encephalitis (13,15); however, emerging evidence suggests that peripheral immune regulators, particularly the gut microbiome (19–21), play an important role in shaping these neuroimmune responses. Clinically, changes in gut microbiome composition elevates seizure risk (22) and drug-resistant epilepsy patients also exhibit compositional differences when compared to drug-sensitive patients (23,24), highlighting a bidirectional cross-talk between the gastrointestinal tract and the brain. Moreover, we previously demonstrated that

experimentally-induced intestinal dysbiosis in the TMEV model alters ASyS burden and produces paradoxical effects on CBZ antiseizure efficacy, with dysbiosis itself being associated with fewer ASyS, while rendering CBZ proconvulsant (1). Together, these findings position the gut microbiome as a key determinant of neuroimmune signaling, which may carry downstream effects on antiseizure medication (ASM)-mediated seizure control in the setting of viral infection-induced ASyS onset. However, few studies have fully explored the bidirectional interactions between the gut-brain axis and ASM treatment on seizure-induced hippocampal neuroinflammation and neuropathology. Therefore, we hypothesized that our previously observed effects of gut dysbiosis on ASyS burden and carbamazepine efficacy (1), impacted neurodegeneration, astrogliosis, and microgliosis following TMEV infection.

The gut microbiome is an understudied contributor to seizure symptoms of epilepsy and therapeutic response, but how experimentally-evoke gut dysbiosis influences neuropathological changes in the context of acute seizures is less clear. We thus sought to extend our earlier study to assess the effects of gut dysbiosis, ASyS history, and CBZ administration (1) on neuropathological hallmarks associated with CNS infection and viral encephalitis-induced seizures. We herein further demonstrate that the gut microbiome dramatically shifts ASyS-induced neuropathological damage after brain infection with TMEV in mice. Notably, we show that gut dysbiosis alters microglial reactivity and proliferation, which is further influenced by repeated CBZ administration during the acute viral infection period. Altogether, this study adds to a growing body of evidence to suggest that the gut microbiome plays an outsized role in seizure-related impacts within the hippocampus.

## Materials & Methods

*Animals*. Mouse brain tissue from our previously published study was used, with detailed experimental methods described in that earlier publication (1). Briefly, male C56BL/6J mice (4-5

weeks old; Jackson Labs) were pretreated with an oral antibiotic cocktail (ABX; ampicillin (1 g/L), metronidazole (1 g/L), neomycin sulfate (1 g/L), and vancomycin (0.5 g/L) dissolved in saline) or saline (SAL) from Day -2 to the infection day (Day 0), then infected with TMEV (20 μL, $3.0 \times 10^5$ PFU, intracerebrally). Then, during the acute infection period, CBZ (20 mg/kg) or vehicle (VEH; 0.5% methylcellulose) was administered twice daily prior to behavioral seizure assessment. All animal use was approved by the University of Washington Institutional Animal Care and Use Committee (protocol 4387-02) and conformed to ARRIVE guidelines (25).

*Histopathology*. Brain tissue was cryosectioned (Leica) at a thickness of 40 μm, mounted on Fisher Superfrost Plus microscope slides (1255015; 4 sections/slide), and stored at 4ºC. Cell death was assessed using Fluoro-Jade C (FJC; Histochem, 2FJC) with Hoechst 33342 nuclear counter stain (Invitrogen, 62249) as we previously published (1,26). We previously assessed FJC qualitatively (yes/no brain samples with FJC positive labeling; (1); thus this present study aimed to quantitatively extend and expand those earlier results . Astroglia proliferation and neuronal proliferation in the hippocampus (CA1, CA3, and dentate gyrus [DG]) were assessed using immunofluorescence (IF) procedures. Slides were washed three times with 0.1 M PBS and blocked in a Triton X solution (0.1% Triton and 1% bovine serum albumin [BSA] in 0.1 M PBS) with 10% goat serum for 2 hours. Tissue was incubated overnight at 4 ºC with primary antibody directed to Ki-67 (Abcam, ab16667, 1:300) diluted in the same Triton X solution used for blocking step. Sections were then rinsed three times in 0.1 M PBS and incubated for 1 hour in goat anti-rabbit secondary conjugated to Alexa Fluor 555 (Abcam, ab150078, 1:500) with anti-GFAP conjugated to Alexa Fluor 488 (Sigma, MAB3402X, 1:1000) or anti-NeuN conjugated to Alexa Fluor 488 (Sigma, MAB377X, 1:300). Finally, microglia proliferation and activation in the hippocampus were assessed using similar IF procedures. Slides were washed three times with 0.3% Triton X in

0.1 M PBS and blocked for 1 hour with the same Triton X solution and 5% BSA. Tissue was incubated overnight at 4 ºC with primary antibodies directed to Ki-67 (ThermoFisher, 14-5698-80, 1:300), Iba-1 (Fujifilm, 019-19741, 1:1000), and CD68 (ThermoFisher, 968-MSM3-P0, 1:1000) diluted with 1% BSA and the 0.3% Triton X solution. Slides were then rinsed in the 0.3% Triton X solution three times and incubated for 2 hours in, respectively, goat anti-rat secondary conjugated to Alexa Fluor 488 (ThermoFisher, A-11006, 1:500), goat anti-rabbit conjugated to Alexa Fluor 555 (Abcam, ab150078, 1:1000), and goat anti-Mouse conjugated to Alexa Fluor 647 (ThermoFisher, A-21235, 1:2000). All IF stained slides were counterstained with DAPI with Prolong Gold (Invitrogen, P36935). Sample sizes varied across experimental groups and stains due to tissue loss during histological processing. Sample sizes utilized for each stain are outlined in

Table 1.

All slides were imaged on an upright fluorescent microscope (Leica DM6 B) with a 20x objective with constant acquisition settings (100 ms exposure, 1x gain). Raw grey scale 16-bit images from the Iba-1, GFAP, FJC, and NeuN channels were utilized to count stain-positive cells using ImageJ Fiji (1.54p). Then Iba-1-, GFAP- and NeuN-positive cells co-labeled with Ki-67 and Iba-1-positive cells co-labeled with CD68 were identified using the colocalization plugin (https://imagej.net/ij/plugins/colocalization.html) and counted using ImageJ. To remove bias in the analysis, an automated macro was created using ImageJ software that performed the following functions to each raw image: each image was first converted to 8-bit, then a Gaussian Blur filter with default sigma settings was applied, next images were thresholded using predetermined settings, and cells were counting using predetermined size parameters. To determine the stain-specific background signal threshold method and range, a subset of images (3 images/treatment

group, 4 images/hippocampal subregion) was selected for each stain. The auto threshold function was run on all subset images whereby all threshold methods were applied using default range settings and the default threshold range for each subset image was recorded. The threshold method with the lowest standard deviation and the average threshold range for that method were utilized for image analysis. Next, particle size parameters were determined by measuring 6 cells across all subset images and the average minimum and maximum measurements across images were utilized. Image analysis parameters for each stain are outlined in Supplementary Table 1.

*Statistical Analysis*. Two-way ANOVA with *post-hoc* Tukey t-tests was used to compare cell counts across TMEV infection groups. Statistical analysis was performed in GraphPad Prism 10 (10.6.1), with $p < 0.05$ considered significant.

## Results

TMEV-infection induced ASyS leads to hippocampal damage and neurodegeneration by 7 days post-infection (13,15). Thus, neuronal death was assessed across hippocampal regions via FJC labeling (Figure 1). ABX-induced gut dysbiosis worsened pyramidal layer neuronal death selectively in CA1 ($F(1,35)=13.37$, $p<0.001$), while CBZ significantly attenuated the dysbiosis-induced increase in neuronal cell death in CA1 ($F(1,35)=14.04$, $p<0.001$), CA3 ($F(1,35)=14.91$, $p<0.001$), and DG ($F(1,35)=17.00$, $p<0.001$). Significant dysbiosis × CBZ interactions also occurred in CA1 ($F(1,35)=12.51$, $p=0.001$) and DG ($F(1,35)=5.127$, $p=0.03$). *Post hoc* comparisons revealed that dysbiotic (i.e., ABX-VEH) mice exhibited greater cell death in CA1 than all other groups ($p<0.0001$), and greater cell death than SAL-CBZ ($p=0.01$) and ABX-CBZ ($p<0.001$) in DG. These results indicate that intestinal dysbiosis exacerbates TMEV-induced hippocampal neurodegeneration while CBZ reverses these effects. Previously, we reported that ABX-induced gut dysbiosis leads to reduced seizure burden in the TMEV model, however, CBZ

was proconvulsant under these conditions (1), indicating that dysbiosis-induced neurodegeneration may have prevented seizure generalization.

Considering the significant microgliosis that occurs with TMEV infection and ASyS presentation (15), we next evaluated microglial phenotypes in hippocampal subregions in dysbiotic and intact mice with and without TMEV infection (Figure 2), including microgliosis, proliferation, and activation.Figure 2 Gut dysbiosis significantly increased microgliosis (Figure 2B) in all hippocampal regions, as indicated by main effects of ABX-induced gut dysbiosis (CA1: $F(1,39)=5.579$, $p=0.02$; CA3: $F(1,39)=11.21$, $p=0.002$; DG: $F(1,39)=14.72$, $p<0.001$) and CBZ administration (CA1: $F(1,39)=14.39$, $p<0.001$; CA3: $F(1,39)=11.21$, $p<0.001$; DG: $F(1,39)=30.30$, $p<0.0001$). Significant dysbiosis x CBZ interactions were also observed in CA1 ($F(1,39)=14.42$, $p<0.001$), CA3 ($F(1,39)=23.24$, $p<0.0001$), and DG ($F(1,39)=37.36$, $p<0.0001$), driven by elevated microgliosis in ABX-VEH mice relative to all other groups (CA1: $p<0.001$; CA3: $p<0.0001$; DG: $p<0.0001$). Microglial proliferation (Figure 2C) followed a similar pattern, with significant main effects of experimentally-induced gut dysbiosis (CA1: $F(1,39)=11.00$, $p=0.002$; CA3: $F(1,39)=9.279$, $p=0.004$; DG: $F(1,39)=9.909$, $p=0.003$) and CBZ (CA1: $F(1,39)=24.98$, $p<0.0001$; CA3: $F(1,39)=14.37$, $p<0.001$; DG: $F(1,39)=22.86$, $p<0.0001$) across all regions. Gut dysbiosis × CBZ interactions were again significant in CA1 ($F(1,39)=16.48$, $p<0.001$), CA3 ($F(1,39)=14.41$, $p<0.001$), and DG ($F(1,39)=18.27$, $p<0.001$), with ABX-VEH mice displaying significantly increased proliferation relative to all other experimental groups (CA1: $p<0.0001$; CA3: $p<0.001$; DG: $p<0.0001$). In contrast, microglial activation (Figure 2D) was selectively affected in the DG, where a significant main effect of ABX-induced dysbiosis ($F(1,22)=4.996$, $p=0.04$) and a dysbiosis × CBZ interaction ($F(1,22)=6.90$, $p=0.02$) occurred. *Post hoc* analysis revealed decreased microglial activation in ABX-CBZ mice relative to SAL-CBZ mice ($p=0.04$), with no significant

effects detected in CA1 or CA3. Together, these findings indicate the gut dysbiosis increases hippocampal microgliosis and microglial proliferation, whereas repeated CBZ administration reversed these effects exclusively in the DG.

Astroglial responses, including astrogliosis and proliferation, were assessed across hippocampal regions (Figure 3). Astrogliosis was significantly affected by ABX-induced dysbiosis in CA3 ($F(1,37)=28.25$, $p<0.0001$) and DG ($F(1,39)=21.56$, $p<0.0001$), but not CA1 ($F(1,36)=4.03$, $p=0.052$), with ABX administration-induced gut dysbiosis being associated with increased astrogliosis in CA3 after TMEV infection, but decreased astrogliosis in DG. CBZ treatment reduced astrogliosis in CA1 ($F(1,36)=5.475$, $p=0.03$) and CA3 ($F(1,37)=28.13$, $p<0.0001$) but had no effect in DG ($F(1,39)=0.72$, $p=0.40$). Dysbiosis × CBZ interactions were significant in CA1 ($F(1,36)=28.48$, $p<0.0001$) and CA3 ($F(1,37)=32.52$, $p<0.0001$), driven by elevated astrogliosis in ABX-VEH mice compared to SAL-VEH (CA1: $p<0.0001$; CA3: $p<0.0001$), SAL-CBZ (CA1: $p=0.02$; CA3: $p<0.0001$), and ABX-CBZ mice (CA1: $p<0.0001$; CA3: $p<0.0001$). Astroglial proliferation (Figure 3C) followed a similar pattern. ABX-induced intestinal dysbiosis increased proliferation in CA1 ($F(1,36)=4.201$, $p=0.04$) and CA3 ($F(1,37)=22.08$, $p<0.0001$), but decreased it in DG ($F(1,37)=9.805$, $p=0.003$), while CBZ reduced proliferation in CA1 ($F(1,36)=8.212$, $p=0.007$) and CA3 ($F(1,37)=24.79$, $p<0.0001$), with dysbiosis × CBZ interactions in the same regions (CA1: $F(1,36)=19.53$, $p<0.0001$; CA3: $F(1,37)=20.43$, $p<0.0001$), driven by elevated proliferation in ABX-VEH mice compared to SAL-VEH (CA1: $p<0.0001$; CA3: $p<0.0001$), SAL-CBZ (CA1: $p=0.008$; CA3: $p<0.0001$), and ABX-CBZ mice (CA1: $p<0.0001$; CA3: $p<0.0001$). DG showed a distinct pattern, with ABX-induced dysbiosis being associated with reduced astroglial proliferation regardless of CBZ treatment ($F(1,37)=9.805$, $p=0.003$). In summary, astroglial proliferation and astrogliosis mirrored

microglial patterns across CA1 and CA3, with ABX-induced gut dysbiosis enhancing these measures and CBZ reversing this profile. Conversely, gut dysbiosis was associated with reduced astroglial activity in the DG of TMEV-infected mice. Altogether, these data suggest that astroglial response was worsened by experimentally induced gut dysbiosis in CA1 and CA3 of dorsal hippocampus, where most of the neuronal death following TMEV infection occurred.

Finally, neuron counts and neuronal proliferation were assessed across hippocampal regions following TMEV infection and experimentally-evoked gut dysbiosis (Figure 4), with minimal differences noted between groups. Evoked intestinal dysbiosis was associated with decreased neuron cell count (Figure 4B) in the DG ($F(1,32)=4.689$, $p=0.04$), but not CA1 or CA3. Meanwhile, neuron proliferation (Figure 4C) showed a significant dysbiosis × CBZ interaction solely in CA1 ($F(1,37)=4.687$, $p=0.04$). However, there were no significant *post hoc* differences in neuronal proliferation in this brain region. Thus, gut dysbiosis decreased neuron cell count in DG but had minimal effects on neuron proliferation in any of the assessed brain regions in this study.

## Discussion

The TMEV model of infection-induced ASyS is a translationally relevant model that is driven by significant peripheral immune system response that can be shaped by the gut microbiome. This study extends our previous work investigating the impact of experimentally-evoked gut dysbiosis on ASyS burden and CBZ antiseizure activity following TMEV infection (1) to now assess the synergistic interaction between ABX-induced gut dysbiosis and CBZ on hippocampal neuropathology. Our present study reveals three distinct histopathological outcomes following gut dysbiosis in the TMEV model: (1) worsened neurodegeneration and inflammation across hippocampal regions; (2) CBZ mitigated these effects; and finally, (3) hippocampal region-

specific changes to neurodegeneration and inflammation. The region-specific changes were most intriguing, with DG exhibiting distinct differences from CA1 and CA3 in microglial activation and astrogliosis in the setting of ABX-induced gut dysbiosis. Importantly, this current investigation provides critical insight into the effects of peripheral immune system priming on CNS pathology in response to an epileptogenic insult, carrying large translational potential to managing clinical ASyS.

Our results demonstrate that ABX-induced dysbiosis exacerbates neurodegeneration and neuroinflammation following TMEV infection. Prior work shows that gut dysbiosis alone promotes both microgliosis (27) and astrogliosis (28), thus identifying a potential mechanism for the peripheral immune cell migration and activation that drives pathological features in this acute seizure model (12,15,29,30). Similarly, following the sustained severe seizures of status epilepticus, microglial activation precedes and worsens astrogliosis (31,32). Astroglial reactivity contributes to seizure generation and epileptogenesis (31,33) through functional alterations, including impaired glutamate uptake (33–35). Moreover, astroglial reactivity is a well-established response to neurodegeneration (36) and contributes to epileptiform activity (37). Consistent with this framework, TMEV infection following ABX-induced intestinal dysbiosis increased astrogliosis, subsequently contributing to neurodegeneration (31,38). Whether dysbiosis worsens the risk of post-infection epileptogenesis in this or other acquired epilepsy models remains to be fully defined.

Despite overall worsened neuroinflammation, gut dysbiosis did not increase microglial activation. Previous studies demonstrate that gut dysbiosis impairs microglial maturation and activation in germ-free mice, conventionalized germ-free mice, and ABX-treated mice (39,40), indicating that microglial function depends on continuous input from a complex gut microbiome.

Although gut dysbiosis did not increase microglial activation in our model, inflammation itself can drive microglial proliferation (41,42), which may further contribute to neurodegeneration (42,43). Importantly, excessive proliferation may impair the transition to an active phagocytic state (43), consistent with our observations. Interestingly, gut dysbiosis confers an anticonvulsant effect in this model (1), suggesting that neurodegeneration may limit seizure generalization while still promoting a neuroinflammatory response (44). Future studies incorporating EEG monitoring will be necessary to determine whether subthreshold epileptiform activity is also present in TMEV-infected mice with experimentally-induced intestinal dysbiosis.

Our prior study suggested that repeated CBZ administration in the setting of gut dysbiosis was associated with a proconvulsant effect, leading us to anticipate an even greater neuropathological response in this follow-on investigation. Contrary to the behavioral outcomes, CBZ administration from 3-7 DPI was associated with reduced microgliosis, astrogliosis, cellular proliferation, and hippocampal neuronal cell death, indicating robust neuroprotective and anti-inflammatory effects, regardless of gut microbiome integrity. Although prior work reported increased astrogliosis following CBZ treatment in the TMEV model (12), CBZ is generally recognized as anti-inflammatory (45–47), including direct suppression of microglial inflammatory responses (48–50). Consistent with this, CBZ attenuated gut dysbiosis-induced neuropathological changes under both dysbiotic and eubiotic conditions. Despite these neuroprotective effects, dysbiotic mice treated with CBZ exhibited increased seizure susceptibility relative to eubiotic counterparts (1). One possibility is that excessive suppression of inflammation resulted in a deficient neuroimmune response, thereby facilitating ASyS (51). Alternatively, gut dysbiosis-induced alterations in pharmacokinetic mechanisms may contribute to this effect. Inflammation is known to inhibit cytochrome P450 enzymes and hepatic drug transporters that regulate drug

metabolism (52). Moreover, intestinal inflammation reduces ASM efficacy while increasing seizure risk (53). However, circulating plasma CBZ concentrations did not differ between groups (1). Together, these findings highlight the need for further investigation into systemic and intestinal inflammatory mechanisms underlying gut dysbiosis-associated alterations in ASM efficacy.

At the hippocampal subregion level, gut dysbiosis produced distinct effects, with the DG exhibiting impaired microglial activation and astrogliosis. Gut dysbiosis reduced astrogliosis in the DG regardless of CBZ treatment, whereas microglial activation was selectively impaired in dysbiotic mice treated with CBZ. Although this pattern may reflect suppression of pathological inflammation by CBZ (51), the absence of broader microglial effects suggests that gut dysbiosis-induced alterations in pharmacokinetic-pharmacodynamic interactions are more likely contributing to this phenotype. The region-specific astroglial responses may instead reflect hippocampal circuit organization, particularly the indirect hippocampal pathway, in which entorhinal cortex inputs project to the DG and propagate through mossy fiber connections with CA3 to CA1 via the Schaffer collateral pathway (54,55). Given the proximity of CA3 to the infection site, astrocytic activation may propagate along this circuit, consistent with sustained astrogliosis in CA3 and CA1, which enhances synaptic activity in these regions (54,56,57). In contrast, DG is further away and upstream from the infection site, likely preventing neuropathological deficits (13). Moreover, DG contains a higher proportion of glutamate-releasing astrocytes that decrease local synaptic activity (58) while facilitating downstream excitation (56). Accordingly, the observed increase in astrogliosis in CA1 and CA3 coupled with reduced astrogliosis in DG may amplify inflammatory and excitatory signaling beyond DG through hippocampal circuitry. Given that reactive astrogliosis increases susceptibility to epileptogenesis (31,38), these region-specific alterations identify a potential circuit-based mechanism contributing

to ASyS following TMEV infection and possibly the later emergence of SRS. Collectively, these findings suggest that astroglia engage hippocampal networks to modulate synaptic activity and ongoing neuroinflammatory signaling, highlighting an underexplored mechanism linking regional neuroinflammation to seizure vulnerability.

Overall, our findings demonstrate the gut dysbiosis exacerbates neuroinflammation and neurodegeneration in a hippocampal region-specific manner in the context of a TMEV infection, despite conferring anticonvulsant effects (1). Differential astrocytic responses across hippocampal subregions suggest that hippocampal circuitry contributes to inflammatory signaling and may influence ASyS presentation, warranting further investigation. Importantly, although gut dysbiosis reduces overt seizure burden, the associated neuropathology indicates a potentially worsened disease trajectory, underscoring the need to evaluate long-term outcomes and subthreshold epileptiform activity using chronic monitoring and video-EEG for SRS. In contrast, CBZ reduced neuroinflammation and cell death, supporting a neuroprotective mechanism underlying antiseizure efficacy in the TMEV model. However, this protection was lost under ABX-induced dysbiotic conditions, highlighting a critical interaction between gut health and ASM activity that occurs independently of circulating plasma concentrations (1). Given evidence that inflammation can disrupt cytochrome P450 activity and drug transport mechanisms (52), elucidating how gut dysbiosis alters pharmacokinetic mechanisms of CBZ and other ASM in this translationally relevant model may reveal novel strategies to optimize seizure control in people with epilepsy.

**Declarations**

***Ethical Publication Statement***

We confirm that we have read the Journal's position on issues involved in ethical publication and affirm that this report is consistent with those guidelines.

***Individual Contributions***

Sophia Shonka, Inga Erickson, Melissa Barker-Haliski: conception or design of the work. Sophia Shonka, Inga Erickson, Melissa Barker-Haliski: acquisition, analysis, or interpretation of data. Sophia Shonka, Inga Erickson, Melissa Barker-Haliski: drafting or substantially revising the work.

***Funding***

This work was supported by the Plein Center for Aging and University of Washington School of Pharmacy

***Disclosures***

None of the authors have any conflict of interest to disclose. We confirm that we have read the Journal's position on issues involved in ethical publication and affirm that this report is consistent with those guidelines

***Data Availability***

All clinical monitoring, behavioral, and histological data is available upon request from the corresponding author.

**References**

1. Erickson I, Davidson S, Choi H, Rho S, Guignet M, Peagler K, et al. Intestinal Dysbiosis Alters Acute Seizure Burden and Antiseizure Medicine Activity in the Theiler's Virus Model of Encephalitis. Epilepsia. 2025 Mar 28;

2. Singh NA, Otto JF, Dahle EJ, Pappas C, Leslie JD, Vilaythong A, et al. Mouse models of human KCNQ2 and KCNQ3 mutations for benign familial neonatal convulsions show seizures and neuronal plasticity without synaptic reorganization. J Physiol. 2008 May 17;2008;586(14):3405-23.

3. Libbey JE, Fujinami RS. Neurotropic Viral Infections Leading to Epilepsy: Focus on Theiler's MurineEncephalomyelitis Virus. Future Virol. 2011 Nov;6(11):1339–50.

4. Annegers JF, Hauser WA, Beghi E, Nicolosi A, Kurland LT. The risk of unprovoked seizures after encephalitis and meningitis. Neurology. 1988;38(9):1407–10.

5. Misra UK, Tan CT, Kalita J. Viral encephalitis and epilepsy. Epilepsia. 2008 Aug;49(s6):13–8.

6. Ba-Diop A, Marin B, Druet-Cabanac M, Ngoungou EB, Newton CR, Preux PM. Epidemiology, causes, and treatment of epilepsy in sub-Saharan Africa. Lancet Neurol. 2014 Oct;13(10):1029–44.

7. Bosak M, Słowik A, Kacorzyk R, Turaj W. Implementation of the new ILAE classification of epilepsies into clinical practice - A cohort study. Epilepsy Behav EB. 2019 Jul;96:28–32.

8. DePaula-Silva AB, Hanak TJ, Libbey JE, Fujinami RS. Theiler's Murine Encephalomyelitis Virus Infection of SJL/J and C57BL/6J Mice: Models for Multiple Sclerosis and Epilepsy. J Neuroimmunol. 2017 Jul 15;308:30–42.

9. Stewart KAA, Wilcox KS, Fujinami RS, White HS. Development of Postinfection Epilepsy After Theiler's Virus Infection of C57BL/6 Mice. J Neuropathol Exp Neurol. 2010 Dec;69(12):1210–9.

10. Barker-Haliski M, Nishi T, White HS. Soticlestat, a novel cholesterol 24-hydroxylase inhibitor, modifies acute seizure burden and chronic epilepsy-related behavioral deficits following Theiler's virus infection in mice. Neuropharmacology. 2022 Nov 8;222(109310).

11. Barker-Haliski M, Heck TD, Dahle EJ, Vanegas F, Pruess TH, Wilcox KS, et al. Acute treatment with minocycline, but not valproic acid, improves long-term behavioral outcomes in the Theiler's virus model of temporal lobe epilepsy. Epilepsia. 2016 Dec;57(12):1958–67.

12. Barker-Haliski M, Dahle EJ, Heck TD, Pruess TH, Vanegas F, Wilcox KS, et al. Evaluating an Etiologically Relevant Platform for Therapy Development for Temporal Lobe Epilepsy: Effects of Carbamazepine and Valproic Acid on Acute Seizures and Chronic Behavioral Comorbidities in the Theiler's Murine Encephalomyelitis Virus Mouse Model. J Pharmacol Exp Ther. 2015 May;353(2):318–29.

13. Umpierre AD, Remigio GJ, Dahle EJ, Bradford K, Alex AB, Smith MD, et al. Impaired cognitive ability and anxiety-like behavior following acute seizures in the Theiler's virus model of temporal lobe epilepsy. Neurobiol Dis. 2014 Apr;64:98–106.

14. Libbey JE, Hanak TJ, Doty DJ, Wilcox KS, Fujinami RS. NBQX, a highly selective competitive antagonist of AMPA and KA ionotropic glutamate receptors, increases seizures and mortality following picornavirus infection. Exp Neurol. 2016;280:89–96.

15. Loewen JL, Barker-Haliski M, Dahle EJ, White HS, Wilcox KS. Neuronal injury, gliosis, and glial proliferation in two models of temporal lobe epilepsy. J Neuropathol Exp Neurol. 2016;75(4):366–78.

16. Gaspard N, Hirsch LJ, Sculier C, Loddenkemper T, van Baalen A, Lancrenon J, et al. New-onset refractory status epilepticus (NORSE) and febrile infection–related epilepsy syndrome (FIRES): State of the art and perspectives. Epilepsia. 2018;59(4):745–52.

17. Guillemaud M, Hanin A, Riviello JJ, Chavez M, Batra A, Berry M, et al. Standard complete blood count to predict long-term outcomes in febrile infection–related epilepsy syndrome (FIRES): A multicenter study. Epilepsia [Internet]. 2025 Aug 22 [cited 2025 Sep 19];n/a(n/a). Available from: https://onlinelibrary.wiley.com/doi/abs/10.1111/epi.18605

18. Sakuma H, Tanuma N, Kuki I, Takahashi Y, Shiomi M, Hayashi M. Intrathecal overproduction of proinflammatory cytokines and chemokines in febrile infection-related refractory status epilepticus. J Neurol Neurosurg Psychiatry. 2015 Jul 1;86(7):820–2.

19. Ding M, Lang Y, Shu H, Shao J, Cui L. Microbiota–Gut–Brain Axis and Epilepsy: A Review on Mechanisms and Potential Therapeutics. Front Immunol. 2021 Oct 11;12:742449.

20. Liu L, Huh JR, Shah K. Microbiota and the gut-brain-axis: Implications for new therapeutic design in the CNS. eBioMedicine. 2022 Mar;77:103908.

21. Agirman G, Yu KB, Hsiao EY. Signaling inflammation across the gut-brain axis. Science. 2021 Nov 26;374(6571):1087–92.

22. Kwack DW, Lee S, Lee DH, Kim DW. Changes in gut microbiome can be associated with abrupt seizure exacerbation in epilepsy patients. Clin Neurol Neurosurg. 2024 Nov;246:108556.

23. Cheraghmakani H, Rezai MS, Valadan R, Rahimzadeh G, Moradi M, Jahanfekr V, et al. Ciprofloxacin for treatment of drug-resistant epilepsy. Epilepsy Res. 2021 Aug 23;176(106742).

24. Peng A, Qiu X, Lai W, Li W, Zhang L, Zhu X, et al. Altered composition of the gut microbiome in patients with drug-resistant epilepsy. Epilepsy Res. 2018 Nov;147:102–7.

25. Sert NP du, Ahluwalia A, Alam S, Avey MT, Baker M, Browne WJ, et al. Reporting animal research: Explanation and elaboration for the ARRIVE guidelines 2.0. PLOS Biol. 2020 Jul 14;18(7):e3000411.

26. Knox KM, Zierath DK, White HS, Barker-Haliski M. Continuous seizure emergency evoked in mice with pharmacological, electrographic, and pathological features distinct from status epilepticus. Epilepsia. 2021;

27. Çalışkan G, French T, Enrile Lacalle S, del Angel M, Steffen J, Heimesaat MM, et al. Antibiotic-induced gut dysbiosis leads to activation of microglia and impairment of cholinergic gamma oscillations in the hippocampus. Brain Behav Immun. 2022 Jan 1;99:203–17.

28. Zhao YF, Wei DN, Tang Y. Gut Microbiota Regulate Astrocytic Functions in the Brain: Possible Therapeutic Consequences. Curr Neuropharmacol. 2021 Aug 11;19(8):1354–66.

29. DePaula-Silva AB. The Contribution of Microglia and Brain-Infiltrating Macrophages to the Pathogenesis of Neuroinflammatory and Neurodegenerative Diseases during TMEV Infection of the Central Nervous System. Viruses. 2024 Jan 13;16(1):119.

30. Kirkman NJ, Libbey JE, Wilcox KS, White HS, Fujinami RS. Innate but not adaptive immune responses contribute to behavioral seizures following viral infection. Epilepsia. 2010 Mar;51(3):454–64.

31. Sano F, Shigetomi E, Shinozaki Y, Tsuzukiyama H, Saito K, Mikoshiba K, et al. Reactive astrocyte-driven epileptogenesis is induced by microglia initially activated following status epilepticus. JCI Insight. 2021 May 10;6(9):e135391.

32. Vezzani A, Ravizza T, Bedner P, Aronica E, Steinhäuser C, Boison D. Astrocytes in the initiation and progression of epilepsy. Nat Rev Neurol. 2022 Dec;18(12):707–22.

33. Maringanti S, Imlay JA. An intracellular iron chelator pleiotropically suppresses enzymatic and growth defects of superoxide dismutase-deficient Escherichia coli. J Bacteriol. 1999 Jun;181(12):3792–802.

34. Coulter DA, Eid T. Astrocytic Regulation of Glutamate Homeostasis in Epilepsy. Glia. 2012 Aug;60(8):1215–26.

35. Peterson AR, Binder DK. Astrocyte Glutamate Uptake and Signaling as Novel Targets for Antiepileptogenic Therapy. Front Neurol. 2020 Sep 8;11:1006.

36. Verkhratsky A, Butt A, Li B, Illes P, Zorec R, Semyanov A, et al. Astrocytes in human central nervous system diseases: a frontier for new therapies. Signal Transduct Target Ther. 2023 Oct 13;8(1):396.

37. Ammothumkandy A, Ravina K, Wolseley V, Tartt AN, Yu PN, Corona L, et al. Altered adult neurogenesis and gliogenesis in mesial temporal lobe epilepsy patients. Nat Neurosci. 2022 Apr;25(4):493–503.

38. Verhoog QP, Holtman L, Aronica E, van Vliet EA. Astrocytes as Guardians of Neuronal Excitability: Mechanisms Underlying Epileptogenesis. Front Neurol [Internet]. 2020 Nov 26 [cited 2025 Dec 31];11. Available from: https://www.frontiersin.org/journals/neurology/articles/10.3389/fneur.2020.591690/full

39. Thion MS, Low D, Silvin A, Chen J, Grisel P, Schulte-Schrepping J, et al. Microbiome Influences Prenatal and Adult Microglia in a Sex-Specific Manner. Cell. 2018 Jan 25;172(3):500-516.e16.

40. Erny D, de Angelis ALH, Jaitin D, Wieghofer P, Staszewski O, David E, et al. Host microbiota constantly control maturation and function of microglia in the CNS. Nat Neurosci. 2015 Jul;18(7):965–77.

41. Färber K, Kettenmann H. Physiology of microglial cells. Brain Res Rev. 2005 Apr 1;48(2):133–43.

42. Gómez-Nicola D, Fransen NL, Suzzi S, Perry VH. Regulation of Microglial Proliferation during Chronic Neurodegeneration. J Neurosci. 2013 Feb 6;33(6):2481–93.

43. Villacampa N, Sarlus H, Martorell P, Bhalla K, Castro-Gomez S, Vieira-Saecker A, et al. Proliferating Microglia Exhibit Unique Transcriptional and Functional Alterations in Alzheimer's Disease. ASN NEURO. 2025 May 19;17(1):2506406.

44. Thergarajan P, Al-Hobaish G, Sutherland G, Tsantikos E, Jupp B, Haskali MB, et al. Early microglia-mediated neuroinflammation after status epilepticus causes behavioral dysfunction and neurocognitive deficits but not epilepsy in mice. Brain Behav Immun. 2026 Jan;131:106183.

45. Popović G, Rakočević S, Čolić M, Kozić L, Drakul M, Mališ V, et al. Anti-inflammatory and immunomodulatory effects of valproate and carbamazepine involve distinct signaling in human peripheral blood mononuclear cells. Immunopharmacol Immunotoxicol. 2025 Jul 4;47(4):553–62.

46. Gómez CD, Buijs RM, Sitges M. The anti-seizure drugs vinpocetine and carbamazepine, but not valproic acid, reduce inflammatory IL-1β and TNF-α expression in rat hippocampus. J Neurochem. 2014;130(6):770–9.

47. Matoth I, Pinto F, Sicsic C, Brenner T. Inhibitory effect of carbamazepine on inflammatory mediators produced by stimulated glial cells. Neurosci Res. 2000 Oct;38(2):209–12.

48. Lauterbach EC. Repurposing psychiatric medicines to target activated microglia in anxious mild cognitive impairment and early Parkinson's disease. Am J Neurodegener Dis. 2016;5(1):29–51.

49. Wang CH, Hsiao CJ, Lin YN, Wu JW, Kuo YC, Lee CK, et al. Carbamazepine attenuates inducible nitric oxide synthase expression through Akt inhibition in activated microglial cells. Pharm Biol. 2014 Nov;52(11):1451–9.

50. Boboc IKS, Cojocaru A, Nedelea G, Catalin B, Bogdan M, Calina D. Chronic Administration of Ion Channel Blockers Impact Microglia Morphology and Function in a Murine Model of Alzheimer's Disease. Int J Mol Sci. 2023 Sep 23;24(19):14474.

51. Löscher W, Howe CL. Molecular Mechanisms in the Genesis of Seizures and Epilepsy Associated With Viral Infection. Front Mol Neurosci [Internet]. 2022 May 9 [cited 2025 Dec 31];15. Available from: https://www.frontiersin.org/journals/molecular-neuroscience/articles/10.3389/fnmol.2022.870868/full

52. Fardel O, Le Vée M. Regulation of human hepatic drug transporter expression by pro-inflammatory cytokines. Expert Opin Drug Metab Toxicol. 2009 Dec;5(12):1469–81.

53. De Caro C, Leo A, Nesci V, Ghelardini C, Di Cesare Mannelli L, Striano P, et al. Intestinal inflammation increases convulsant activity and reduces antiepileptic drug efficacy in a mouse model of epilepsy. Sci Rep. 2019 Sep 27;9(1):13983.

54. Squires A, Park J. Emerging roles of astrocytes in hippocampal circuitry and behavior. Front Cell Neurosci [Internet]. 2025 Nov 21 [cited 2025 Dec 31];19. Available from: https://www.frontiersin.org/journals/cellular-neuroscience/articles/10.3389/fncel.2025.1694643/full

55. Basu J, Siegelbaum SA. The Corticohippocampal Circuit, Synaptic Plasticity, and Memory. Cold Spring Harb Perspect Biol. 2015 Nov 2;7(11):a021733.

56. Adamsky A, Kol A, Kreisel T, Doron A, Ozeri-Engelhard N, Melcer T, et al. Astrocytic Activation Generates De Novo Neuronal Potentiation and Memory Enhancement. Cell. 2018 Jun 28;174(1):59-71.e14.

57. Haustein MD, Kracun S, Lu XH, Shih T, Jackson-Weaver O, Tong X, et al. Conditions and constraints for astrocyte calcium signaling in the hippocampal mossy fiber pathway. Neuron. 2014 Apr 16;82(2):413–29.

58. Martínez-Gallego I, Coatl-Cuaya H, Rodriguez-Moreno A. Astrocytes mediate two forms of spike timing-dependent depression at entorhinal cortex-hippocampal synapses. Calakos N, Chen L, editors. eLife. 2024 Nov 14;13:RP98031.

## Figure and Tables

**Figure 1.** Neuronal cell death level change in the hippocampus of male C57BL/6J mice with and without experimentally-evoked intestinal dysbiosis (SAL or ABX) 7 days after an acute TMEV infection and subsequent administration of the antiseizure medicine, carbamazepine (CBZ, 20 mg/kg, i.p., bid). A) Representative photomicrographs from the CA1 hippocampal subregion of FJC+ cells (green) with Hoechst 33342 nuclear counterstain (blue). B) Experimentally-evoked gut dysbiosis in TMEV-infected mice is associated with increased neuronal cell death in CA1 and DG regions of the hippocampus 7 days post-infection while CBZ treatment is associated with decreased neuronal cell death across hippocampal regions 7 days post-infection. *, $p < 0.05$, **, $p < 0.01$, ***, $p < 0.001$, ****, $p < 0.0001$. Graphs show mean ± SEM, scale bar = 100 µm.

**Figure 2.** Microgliosis, microglial proliferation, and microglial activation level change in the hippocampus of male C57BL/6J mice with and without experimentally-evoked gut dysbiosis (SAL or ABX) 7 days following an acute TMEV infection and subsequent administration of the antiseizure medicine, carbamazepine (CBZ, 20 mg/kg, i.p., bid). A) Representative photomicrographs from the CA1 hippocampal subregion of Iba-1+ (red), Ki-67+ (green), and CD68+ (teal) cells with DAPI nuclear counterstain (blue). B) Experimentally-evoked gut dysbiosis in TMEV-infected mice is associated with increased microgliosis, as measured by increased Iba-1 immunoreactivity, across hippocampal regions. Meanwhile, CBZ treatment reduced microgliosis, regardless of gut dysbiosis status, 7 days following infection. C) Similarly, gut dysbiosis is associated with increased microglial proliferation, as measured by increased Ki-67 immunoreactivity, across hippocampal regions while CBZ treatment is associated with reduced microglial proliferation. D) CBZ administration in TMEV-infected mice with gut dysbiosis led to

decreased microglial activation 7 days post-infection, as measured by reduced CD68 immunoreactivity. *, $p < 0.05$, ***, $p < 0.001$, ****, $p < 0.0001$. Graphs show mean ± SEM, scale bar = 100 µm.

**Figure 3.** Astrogliosis and astroglial proliferation level change in the hippocampus of male C57BL/6J mice with and without experimentally-evoked intestinal dysbiosis (SAL or ABX) 7 days after an acute TMEV infection and subsequent administration of the antiseizure medicine, carbamazepine (20 mg/kg, i.p., bid). A) Representative photomicrographs from the CA1 hippocampal subregion of GFAP+ (green) and Ki-67+ (red) cells with DAPI nuclear counterstain (blue). B) Experimentally-evoked gut dysbiosis in TMEV-infected mice is associated with increased astrogliosis in CA1 and CA3 and decreased astrogliosis in DG 7 days later, as measured by GFAP immunoreactivity. C) Similarly, gut dysbiosis is associated with increased astroglial proliferation in CA1 and CA3 and decreased proliferation in DG, as measured by Ki-67 immunoreactivity. *, $p < 0.05$, **, $p < 0.01$, ****, $p < 0.0001$. Graphs show mean ± SEM, scale bar = 100 µm.

**Figure 4.** Neuronal proliferation level change in the hippocampus of male C57BL/6J mice with and without experimentally-evoked intestinal dysbiosis (SAL or ABX) 7 days after an acute TMEV infection and subsequent administration of the antiseizure medicine, carbamazepine (CBZ, 20 mg/kg, i.p., bid). A) Representative photomicrographs from the CA1 hippocampal subregion of NeuN+ (green) and Ki-67+ (red) cells with DAPI nuclear counterstain (blue). Overall, neither experimentally-evoked gut dysbiosis nor CBZ treatment impacted neuron levels (B) or proliferation (C) in the hippocampus of TMEV-infected mice. Graphs show mean ± SEM, scale bar = 100 µm.

**Table 1.** Summary of Numbers of Animals Used for Each Stain.

| Experimental Group | FJC | Iba-1 & Ki-67 | GFAP & Ki-67 | NeuN & Ki-67 | Iba-1 & CD68 |
|---|---|---|---|---|---|
| SAL-VEH | 11 | 12 | 11 | 13 | 8 |
| SAL-CBZ | 7 | 8 | 8 | 8 | 3 |
| ABX-VEH | 7 | 8 | 8 | 8 | 3 |
| ABX-CBZ | 12 | 13 | 12 | 13 | 9 |

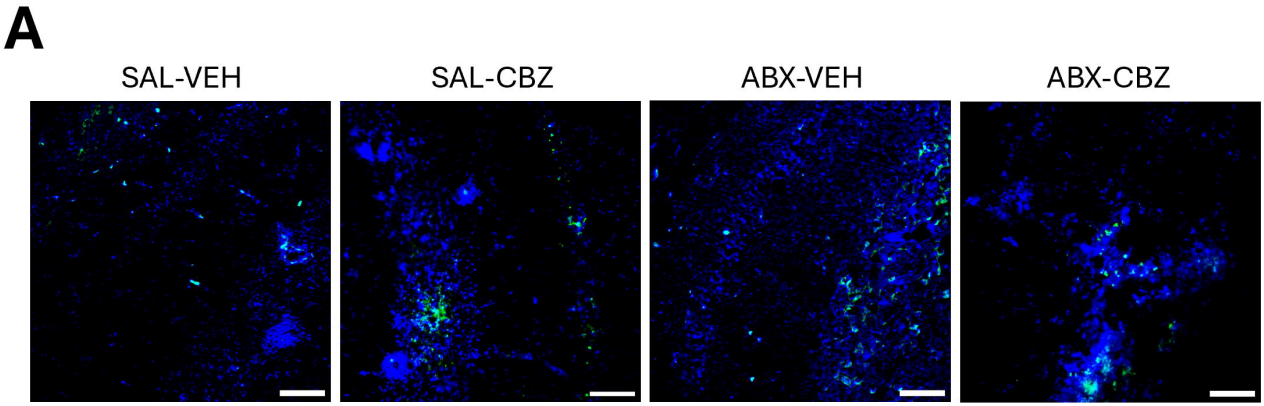


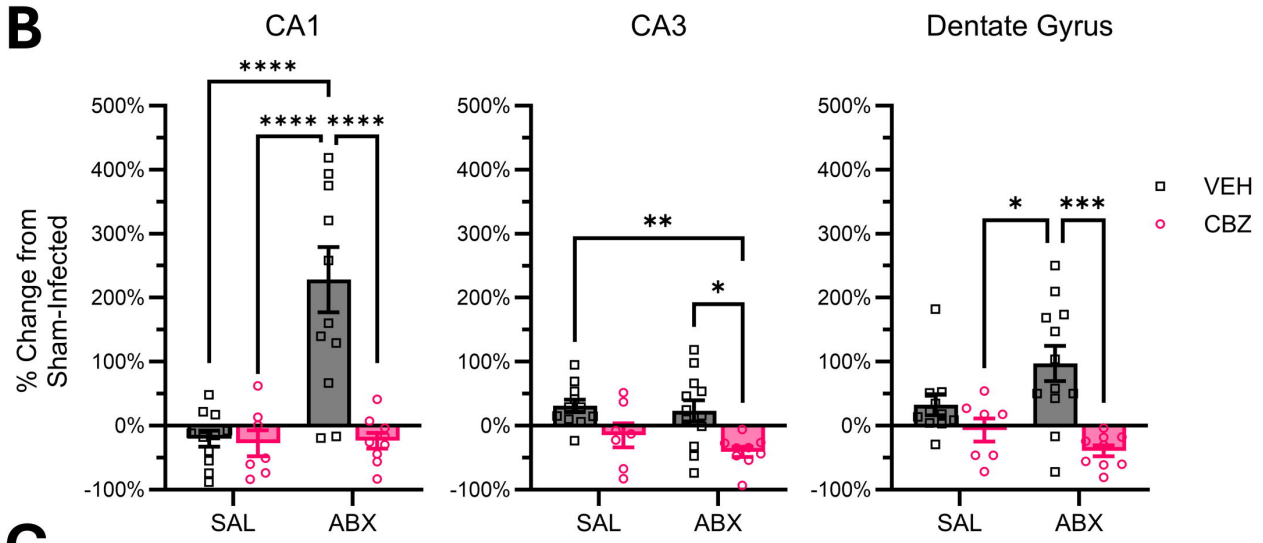


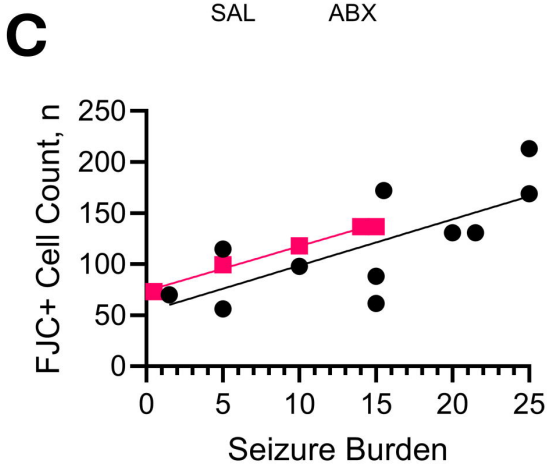


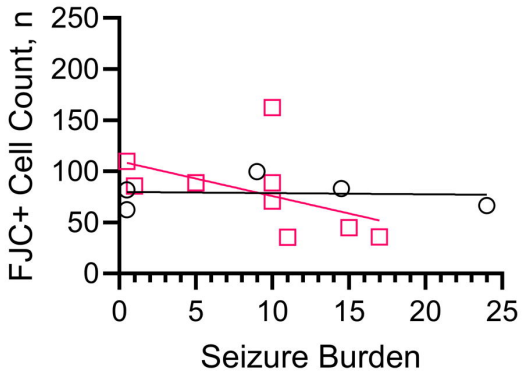


| | SAL-VEH | ABX-VEH |
|---|---|---|
| $R^2$ | 0.540 | 0.989 |
| ***p*-value** | 0.01* | 0.0005*** |

| | SAL-CBZ | ABX-CBZ |
|---|---|---|
| $R^2$ | 0.006 | 0.241 |
| ***p*-value** | 0.903 | 0.149 |

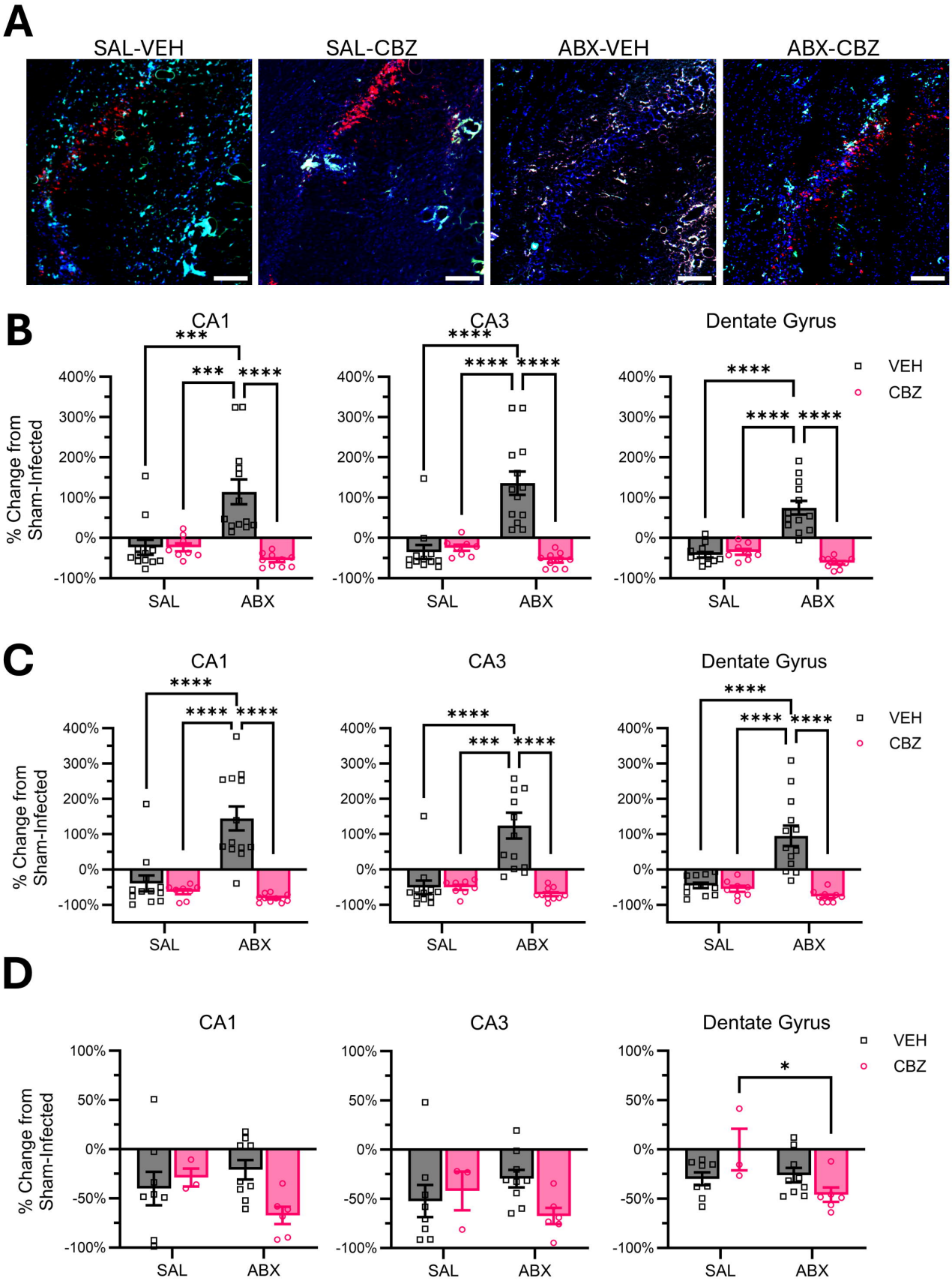
A
SAL-VEH
SAL-CBZ
ABX-VEH
ABX-CBZ
B
CA1
CA3
Dentate Gyrus
% Change from Sham-Infected
400%
300%
200%
100%
0%
-100%
SAL
ABX
VEH
CBZ
***
****
C
D
-50%
50%
*

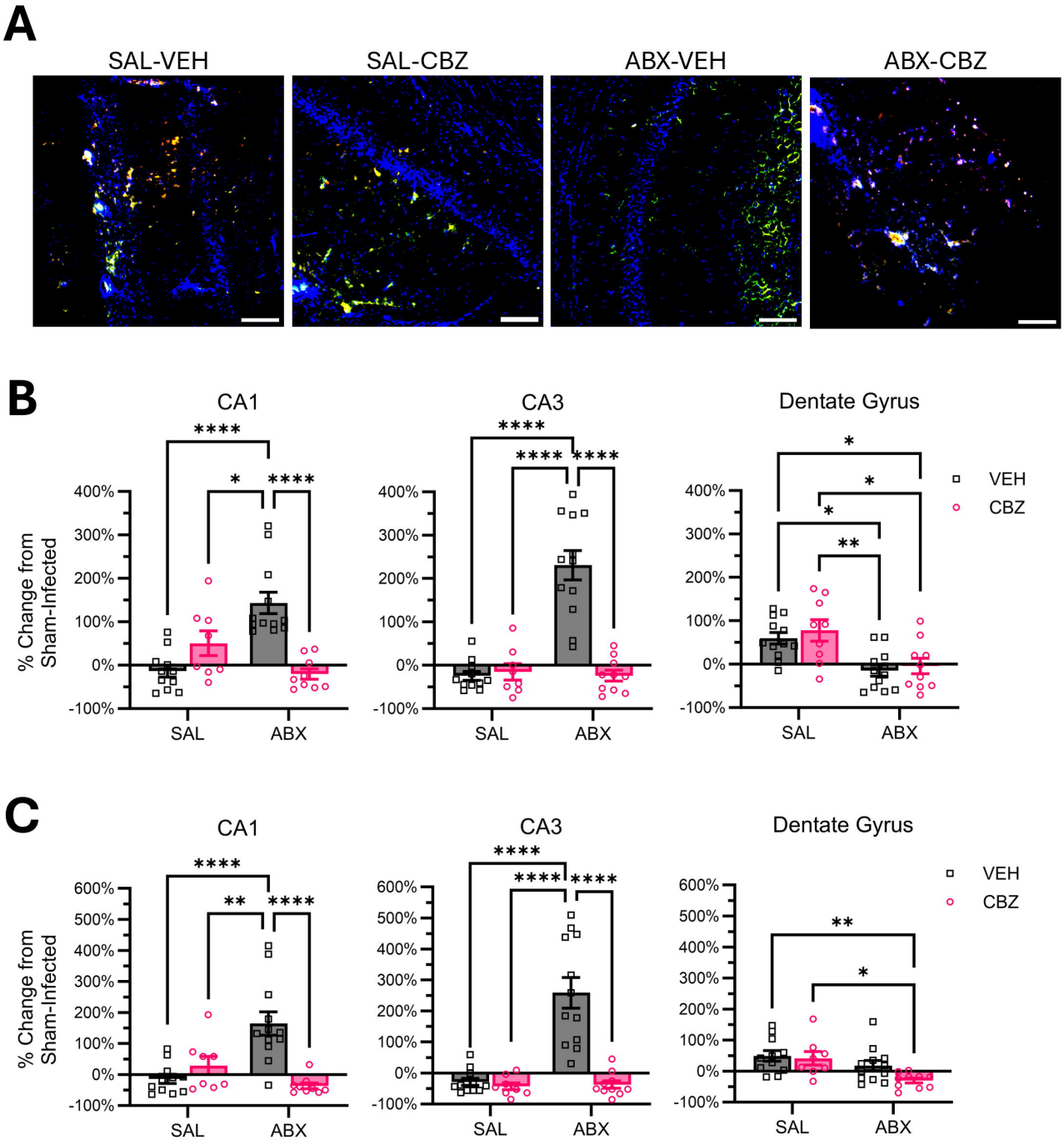
A
SAL-VEH
SAL-CBZ
ABX-VEH
ABX-CBZ
B
CA1
CA3
Dentate Gyrus
% Change from Sham-Infected
400%
300%
200%
100%
0%
-100%
SAL
ABX
VEH
CBZ
C
600%
500%

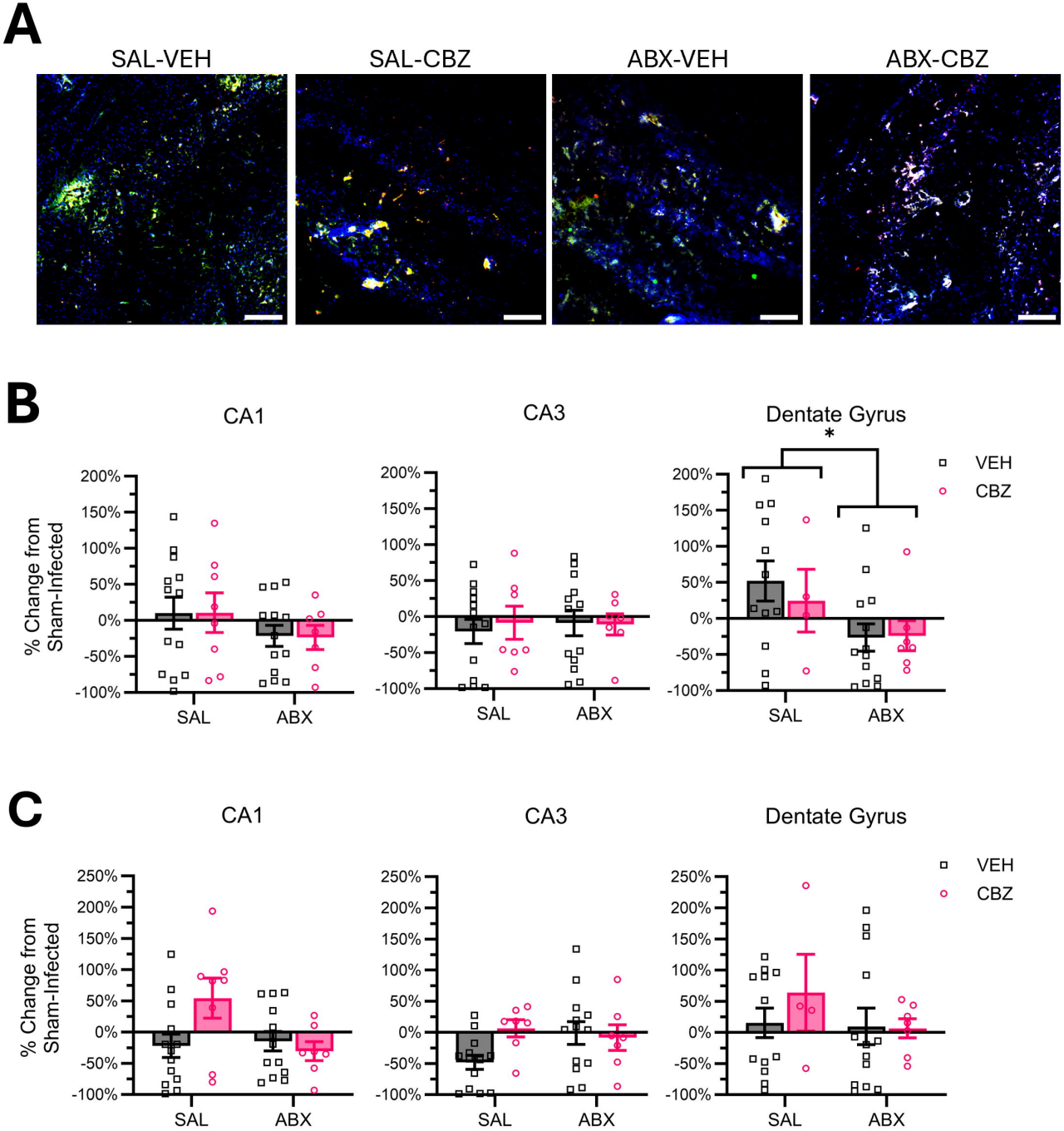
A
SAL-VEH
SAL-CBZ
ABX-VEH
ABX-CBZ
B
CA1
CA3
Dentate Gyrus
*
VEH
CBZ
% Change from Sham-Infected
200%
150%
100%
50%
0%
-50%
-100%
SAL
ABX
C
CA1
CA3
Dentate Gyrus
VEH
CBZ
% Change from Sham-Infected
250%
200%
150%
100%
50%
0%
-50%
-100%
SAL
ABX